HOW TO TELL RIGHT FROM LEFT

Yaakov Hel-Or
Shmuel Peleg
Hagit Zabrodsky

Department of Computer Science
The Hebrew University of Jerusalem
91904 Jerusalem, Israel

Abstract

Many natural shapes have chirality (or handedness): for instance our hands have a right-hand version and a left-hand version, the two types being mirror images of each other. In chemistry, for example, molecules and crystals are classified as having chirality D or L. Interaction between molecules is dependent on their chirality, and chirality may determine chemical characteristics. For instance, only glucose of D-chirality is sweet, while glucose of L-chirality is tasteless.

We study the notion of chirality for two dimensional binary shapes, and introduce measures to test whether a shape is symmetric, and if not whether it is left-handed or right-handed. The measures are based on boundary analysis, and perform well even when digital images of left-handed shapes differ from the mirror images of right-handed shapes. Such situations may occur due to natural variations and digitization errors. The measures can also successfully treat partially occluded shapes, and provide indications on the change of chirality as resolution changes.

1. Introduction

Not only body parts have right or left handedness, this property, *chirality* , exist almost everywhere. Chirality has special significance in the study of elementary particles [1] whose chirality is due to their spin. Likewise molecules can appear in two possible configurations, called D (dextro) chirality and L (levo) chirality [2], each having different characteristics. For instance, glucose of D-chirality is sweet, whereas glucose of L-chirality is tasteless. The first to observe the importance of chirality in chemistry were the French chemists Louis Pasteur (1822-1895) and Jean Baptiste Biot (1774-1862) who determined the connection between crystal's chirality and the deflection of the plane of polarization light passing through them [3].

One property that characterizes chirality is that an object can not be superimposed on its mirror image using translation and rotation. A right hand will never be similar to a left hand unless we look at one of them through a mirror. Thus, the set of all human hands can be divided into two classes, each having its own specific chirality.

The goal of our work is to examine a set of two dimensional shapes, and reveal whether the objects in the set are chiralic. Once shapes are found to be chiralic, we would like to classify them according to chirality class. Theoretically, it is enough to check whether an object has a reflective symmetry, as

chirality is a form of asymmetry. However, almost no real object is exactly symmetric, especially after digitization, therefore we must determine weather the lack of symmetry is a dominant characteristic of the object.

Figure 1 exhibits some intuitive properties of this analysis. Shape A_1 is symmetric and non chiral since its mirror image, A_2, can be superimposed on it by using translation and rotation. Shape B_1, which is obtained by shortening one arm of A_1, is chiral. Shape C_1, with an even shorter arm, is also chiral to a greater degree than B_1. Shortening the arm completely to produce the straight line D_1 results in a symmetric shape again.

The rest of this section is devoted to some basic definitions. Sections 2 and 3 are a review of conventional approaches that seemed theoretically appealing for chirality analysis but were not successful. Section 4 describes our new approach to measure chirality.
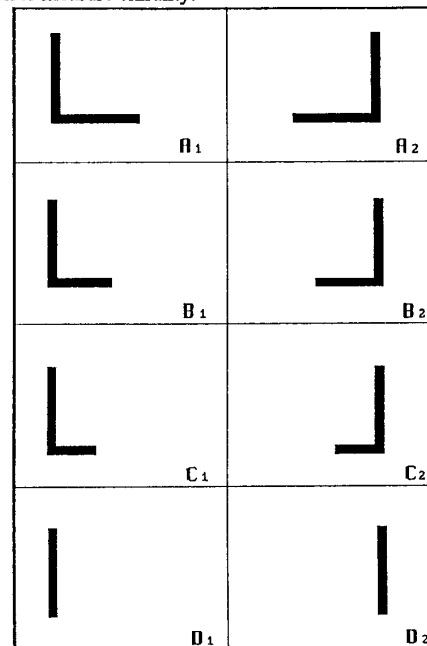

Figure 1:
Shape A_1 is symmetric, B_1 is chiral, C_1 even more chiral, and D_1 is symmetric.

1.1. Chirality

Let $\mathbb{R}$ be the set of points in the plane, and let $K \subseteq \mathbb{R}$ be a set of points. K will be called *chiral* iff there are no reflection σ, translation τ, and rotation δ such that $\delta\tau\sigma(K) = K$. In other words: K is chiral iff it cannot be superimposed on its mirror image using only translation and rotation.

Let K be a chiral set, and let $\sigma(K) = K'$, i.e. K' is the mirror image of K. K and K' are called *enantiomers* and cannot be superimposed on each other.

1.2. Symmetry

K is *symmetric* iff there exist an isometry, which is not the identity, that transforms K onto itself (An isometry is a distance preserving transformation). Therefore, a set which is not chiral is symmetric.
K is *asymmetric* iff there is no isometry that transforms K onto itself.
K is *dissymmetric* iff there is no reflection that transforms K onto itself.

Note: A set is chiral iff it is asymmetric or at least dissymmetric. There are shapes, like the letter Z, that are symmetric, dissymmetric and chiral.

1.3. Centroid

Let $\chi: \mathbb{R} \to \{0,1\}$ be the characteristic function of the set $K \subseteq \mathbb{R}$,

$$\chi(x,y) = \begin{cases} 1 & \text{if } (x,y) \in K \\ 0 & \text{otherwise} \end{cases}$$

The *centroid* of K, (x_0, y_0), is the point such that

$$x_0 = \frac{\sum \chi(x,y)x}{\sum \chi(x,y)} \quad ; \quad y_0 = \frac{\sum \chi(x,y)y}{\sum \chi(x,y)}$$

where the summations above are over the entire plane.

It can be shown that a set K is not chiral iff there is a reflection σ that maps K onto itself. In this case the reflection is about a line that passes through the centroid of K.

2. Moments

The basic approach of using moments for shape analysis is developed by Hu [4]. Using the fact that a set is not chiral iff it is a reflection of itself about a line that passes through its centroid, we look for such a line. Since the centroid can be found easily, we only need to find the angle of this line, and then check the reflection about it.

Given the characteristic function $\chi(x,y)$, its M_{ij} moment is defined by

$$M_{ij} = \sum_{x,y} \chi(x,y)x^i y^j$$

We can find the centroid using $x_0 = \frac{M_{10}}{M_{00}}$, $y_0 = \frac{M_{01}}{M_{00}}$.

From now on we assume that the origin is in the centroid. If the axis of reflection coincides with the y-axis then $M_{ij} = 0$ for odd i since $\chi(x,y) = \chi(-x,y)$. If the reflection axis coincides with the x-axis then $M_{ij} = 0$ for odd j. We will therefore rotate the shape about its origin until $M_{11} = 0$. In this case, if the set is symmetric, either the x-axis or the y-axis is the axis of reflection.

The effect of rotation by θ on M_{11}, yielding M'_{11}, can be shown to be

$$M'_{11} = \cos\theta (M_{02}\sin\theta + M_{11}\cos\theta) - \sin\theta(M_{20}\cos\theta + M_{11}\sin\theta)$$

Looking for θ such that $M'_{11} = 0$ we get

$$\tan(2\theta) = \frac{2M_{11}}{M_{20} - M_{02}} \tag{1}$$

The axis we get after moving the origin to the centroid, and then rotating by θ found in (1) is called the *principal-axis*. If the set is symmetric, it is now symmetric in respect to the x-axis or the y-axis, as $M'_{12} = 0$. If M'_{12} is very small then the y-axis is probably the reflection axis, and if M'_{21} is very small then the x-axis is probably the reflection axis (for exact symmetry either M'_{21} or M'_{12} equals zero). We can now measure the symmetry using correlation. If we assume that the y-axis is the axis of reflection, the measure is

$$W = \frac{\sum_x \sum_y (\chi^2(x,y) - \chi(x,y)\chi(-x,y))}{\sum_x \sum_y \chi^2(x,y)} \tag{2}$$

$W = 0$ indicates symmetric objects, and higher values (maximaly 1) indicate increased chirality.

Using expression (2) we can theoretically find chiral objects, but the results of this method on several shapes were found to be unreliable. Although theoretically the results should be accurate, in practice we used digitized images so that the results were not stable, and the method was found not to be robust. Furthermore, this analysis does not distinguish between enantiomers.

3. Transform Approach

Bigun and Granlaund [5] introduced a transform whose basis functions are spirals, with varying number of "arms" and curvature. Some of the basis functions are shown in Figure 2. As spirals are chiral, they can be used to measure chirality. Left spirals and right spirals have opposing chirality, while the border situation of "spirals" with straight hands is symmetric. Before describing the approach in detail we will mention that it is applicable to grey-level images as well as to binary images.

We will transform the shape $\chi(x,y)$ into polar representation,

$$\chi'(r,\theta) = \chi(r\cos\theta, r\sin\theta)$$

From now on we will represent our shape by a polar representation.
Let Ω be a filled circle of radius R, and let $f(r,\theta)$ and $g(r,\theta)$ be two functions on Ω. We define the scalar product of f and g, $<f,g>$, by

$$<f,g> = \frac{1}{2\pi R} \int_0^{2\pi} \int_0^R f^*(r,\theta)g(r,\theta)d\theta dr$$

We use the following set as the basis functions:

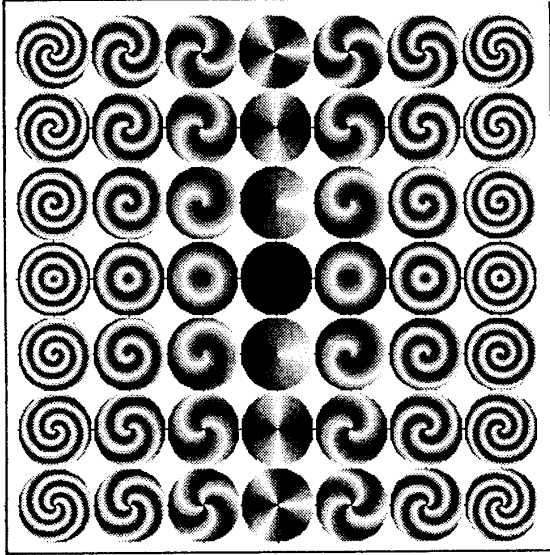$$\Phi_{mn}(r,\theta) = e^{i(mwr + n\theta)} \tag{3}$$

Figure 2:
Bigun's basis functions

where m, n are integers, and $w = \frac{2\pi}{R}$. This set is the one shown in Figure 2, and its arguments are as follows:

n - represents the number of arms.

m - represents the curvature of the arms.

$sgn(m \cdot n)$ - represents the direction of curvature (left spiral vs. right spiral). Due to this feature we need only consider $n > 0$.

The set (3) is a complete orthogonal set, and any continuous function on Ω can be represented by a weighted sum of its members. Φ_{mn} is actually the Fourier functions over the r, θ domain.

Let $f(r, \theta)$ be our shape function on Ω after we have transformed it into polar representation; then we can write

$$f(r, \theta) = \sum_{m,n} C_{mn} \Phi_{mn}(r, \theta)$$

where

$$C_{mn} = <f, \Phi_{mn}> = \frac{1}{2\pi R} \int_0^{2\pi} \int_0^R f(r, \theta) e^{i(mwr + n\theta)} d\theta dr$$

We use the coefficients C_{mn} to analyse an object's chirality after normalizing the image function such that for pure spirals, where $f(r, \theta) = a\Phi_{kl} + b$, then $C_{kl} = 1$ and all other C's are zero.

The following points should be noted:

- The results depend strongly on the choice of origin. Since we know that if an object is symmetric the symmetry axis passes through its centroid, we will use the centroid as the origin.
- The coefficients C_{mn} are complex. By using their magnitude, and neglecting the phase, the results are rotation invariant.

To find the chirality with respect to the origin we use the average of n and m weighted by C_{mn}:

$$M = \frac{\sum_m \sum_n |C_{mn}| m}{\sum_m \sum_n |C_{mn}|} \qquad N = \frac{\sum_m \sum_n |C_{mn}| n}{\sum_m \sum_n |C_{mn}|} \qquad (4)$$

$abs(M)$ represents the magnitude of the chirality.
$sgn(M)$ represents the direction of the chirality.
N indicates the rotational symmetry as represented by the average number of arms.

This method was tried on a number of samples, but the results were unsatisfying. We found that noise disturbed the results. Further, the conversion into polar coordinates of a grid sampled image gave rise to inaccuracies.

4. Rotational Chirality Measures

Features based on object rotation can be used for chirality analysis. As clockwise rotation of an object is identical to counterclockwise rotation of its mirror image, non-chiral objects, which are identical to their mirror-image, will exhibit indifference to the direction of rotation. Chiral objects, on the other hand, will behave differently for the two directions of rotation.

In our scheme we use the following idea: imagine the object as rotating in a medium full of tiny particles. Some boundary segments will "collect" particles. We will use the length of these segments as a feature for chirality analysis. An ideal spiral, for example, rotated in one direction will have no "collecting" points, while rotation in the other direction will have all it's points "collecting". We will initially perform the rotation around the centroid, but eventually use other points. The choice of the center of rotation will be discussed later.

4.1. Boundary Based Measures

Let K be a set of points (pixels), and let E be the set of edge pixels of K, $E \subseteq K$. We will use subsets of the edge pixels that "collect" particles, RGP (right-grasp-pixels) and LGP (left-grasp-pixels), to define chirality measures. We assume that K is simply connected, and define the following:

Let $\{e_i\}_{i=1}^k$ be the sequence of boundary pixels ordered by following the boundary so that the object is to right [6], as in Figure 3. Let O be the axis of rotation. For a boundary pixel e_i we define:

- $\vec{r}_i$: the vector from O to e_i.
- d_i : the length of $\vec{r}_i$.
- θ_i : the angle between $\vec{r}_i$ and the x-axis.
- Δd_i : $d_{(i+1) \mod k} - d_i$, the change in distance from O between e_i and e_{i+1}.
- $\Delta \theta_i$: $\theta_{(i+1) \mod k} - \theta_i$, the change in θ between $\vec{r}_i$ and $\vec{r}_{i+1}$, the angle (e_i, O, e_{i+1}).

We represent the angles in the range $-\pi < \Delta\theta_i, \theta_i \leq \pi$. Figure 3 shows these definitions. Δd_i and $\Delta \theta_i$ can be positive, negative, or zero. When smoothing is desired, we can use $\Delta d_i = (d_{i+1} - d_{i-1})/2$ and $\Delta\theta_i = (\theta_{i+1} - \theta_{i-1})/2$.
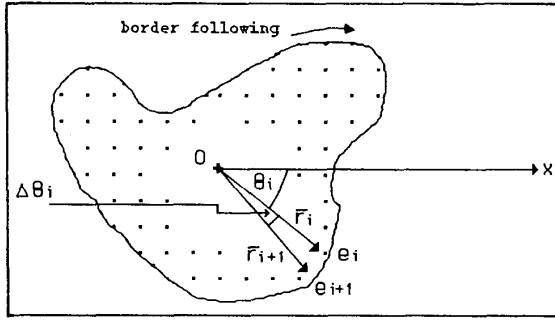
Figure 3:
    some definitions on boundary pixels.

A boundary segment between e_i and e_{i+1} will be on the front edge, encountering particles in clockwise rotation, only if $\Delta d_i < 0$ (Figures 4.C 4.D) and in counter-clockwise rotation when $\Delta d_i > 0$ (Figures 4.A 4.B) The centrifugal power will push the particles away from the axis of rotation, unless the boundary itself serves as an obstacle when $\Delta\theta_i > 0$ (Figures 4.A 4.C). We therefore have

$$LGP = \{ e_i \mid \Delta\theta_i > 0 \ , \ \Delta d_i > 0 \} \qquad (5)$$

$$RGP = \{ e_i \mid \Delta\theta_i > 0 \ , \ \Delta d_i < 0 \}$$

and we notice that $RGP \cap LGP = \varnothing$, and $LGP \cup RGP \subseteq E$. In practice we do not use only the signs of $\Delta\theta_i$ and Δd_i as in definition (5) since it can have very noisy behavior for small values. Therefore, for a given thresholds ε_1 and ε_2 we determine

$$LGP = \{ e_i \mid \Delta\theta_i > \varepsilon_1/d_i \ , \ \Delta d_i > \varepsilon_2 \} \qquad (6)$$

$$RGP = \{ e_i \mid \Delta\theta_i > \varepsilon_1/d_i \ , \ \Delta d_i < \varepsilon_2 \}$$

As chirality measure we use the measure

$$Z = \frac{|LGP| - |RGP|}{|E|} \qquad (7)$$

where the normalization by $|E|$ serves to make the measure independent of size but dependent on the ratio of grasp-pixels to edge-pixels.

In order to develop another measure we adopt the idea of torque, which is force times the distance from the axis. Following this paradigm we can get a slightly different chirality measure: Let $L = \sum_{i \in LGP} d_i$, and $R = \sum_{i \in RGP} d_i$, then a chirality measure will be

$$Z' = \frac{L - R}{\sum_{i \in RGP, LGP} d_i} \qquad (8)$$

Figure 5 shows measures (7) and (8) applied to several shapes, when the centroid is used as the rotation axis.
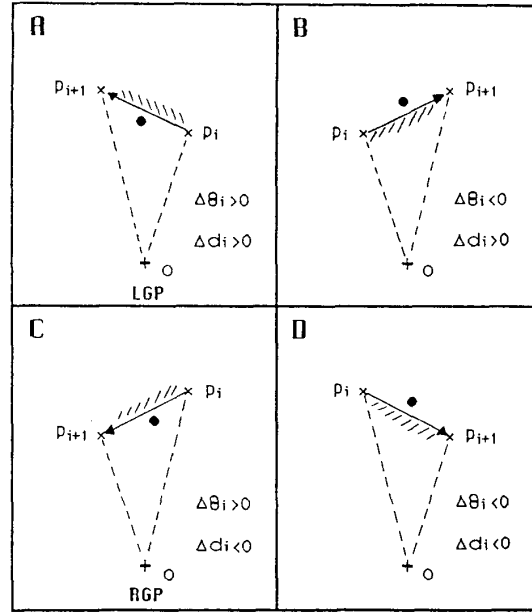

Figure 4:
    properties of boundary particles in rotation.
    4.A - Edge encountering and grasping particles in counter-clockwise rotation (LGP).
    4.B - Edge encountering but pushing away particles in counter-clockwise rotation.
    4.C - Edge encountering and grasping particles in clockwise rotation (RGP).
    4.D - Edge encountering but pushing away particles in clockwise rotation.

Notice that the shape in Figure 5.c is chiral, but since $|LGP| = |RGP|$ measure (7) fails to find its chirality, while measure (8) succeeds.

When we apply measure (7) to a series of shapes as in Figure 1 above, we obtain the predicted results which are shown in Figure 6. In Figure 6, (a) and (d) are not chiral, and indeed have minimum chirality measure. Examples (b) and (c) are both chiral, where (c) has more chirality than (b), and this effect too is reflected in the computed measurements.

4.2. Center of Chirality

Any chirality measure is greatly dependent on the choice of the axis of rotation. The centroid has initially been used as axis of rotation, but this choice can be misleading in some cases, especially for partially occluded shapes. Even for a spiral the centroid will not be the center of the spiral, as shown in Figure 7. We therefore define the following :
center of chirality is a point that maximize the rotational chirality measure ((7) in absolute value) when used as a rotation axis. Figure 7 shows the center of chirality for several shapes. It finds the correct center of the spiral, as well as the real center of some partially occluded shapes.
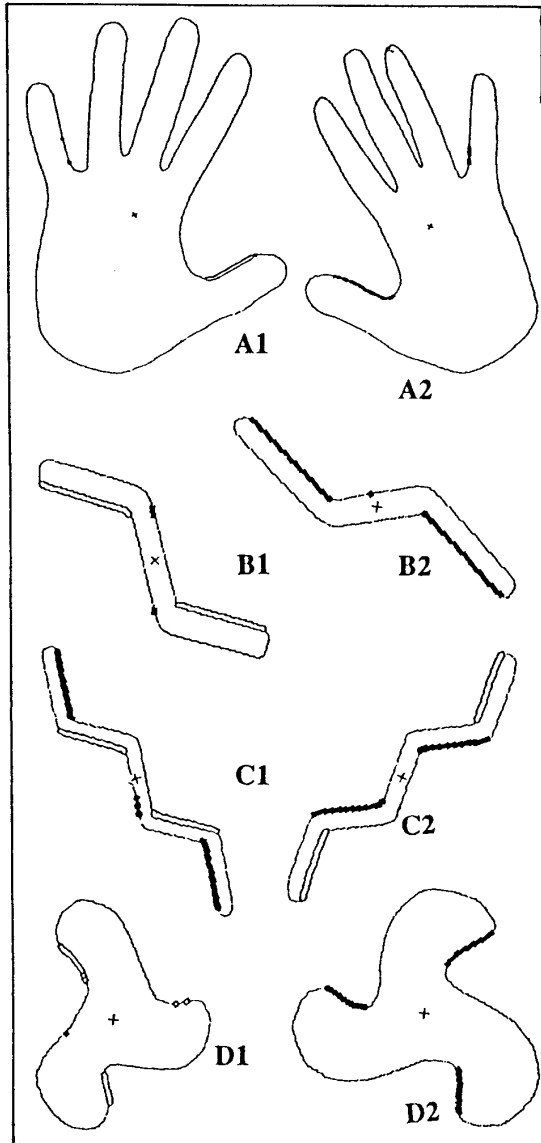
Figure 5:
Application of different rotational chirality measures on several shapes. The black squares $\in RGP$ and the white squares $\in LGP$.

picture	measure (7)	measure (8)
A1	0.02	0.88
A2	-0.02	-0.80
B1	0.26	0.94
B2	-0.27	-0.97
C1	-0.04	-0.25
C2	-0.01	0.23
D1	0.10	0.97
D2	-0.16	-1.00

Figure 6:
Application of measure (7) to a series of shapes around the centroid.

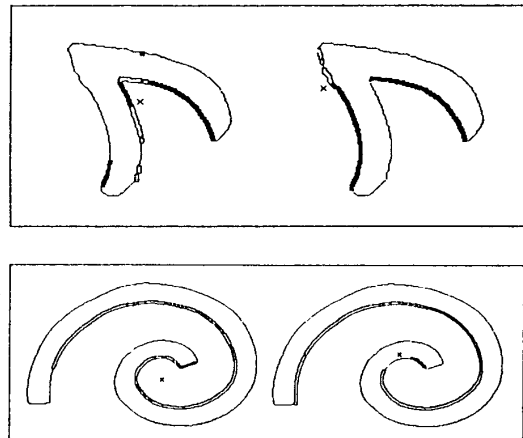| picture	chirality-measure (7)
(a)	-0.001584
(b)	-0.005445
(c)	-0.006369
(d)	0.0

Figure 7:
The center of chirality (left) and the centroid (right) of some shapes

In order to reduce the computational complexity involved in the computation of the center of chirality, and avoid computing the chirality around every point of the image, several heuristics can be used. We could, for example, start searching for the maximal chirality at the centroid, examine a small neighborhood of the current location, and move to the pixel of highest chirality. This iterative search will stop when a point has higher chirality than all its neighbors. Simulated Annealing [7] can be used to

prevent stopping at local maxima. A faster method to reach the center of chirality uses a multiresolution approach, and is discussed in the following section.

5. Multiresolution Approach

Define a pyramid [8] as a sequence of reduced resolution images. The lowest level of the pyramid, L_0, will be the original image of side length 2^N. L_1 will be a reduce image, having a side length of 2^{N-1}, etc. We use the pyramid multiresolution structure for speeding-up the computation and for measuring resolution-dependent chirality information.

The computation of the center of chirality in the pyramid is very fast. We start by computing the center of chirality at a high level using exhaustive search. This is very fast, as such level has only a small number of pixels. Let e_i be the center of chirality at level i. The center of chirality at level $i-1$ can now be computed by projecting e_i into level L_{i-1}, and searching for maximum chirality only in a small neighborhood around this projection. The speed-up introduced in this manner is of order $O(2^{2N})^2$, and uses the assumption that details added between levels L_i and L_{i-1} can change the location of the center of chirality only by a limited distance.

Computing the chirality measure at all resolution levels not only speeds up computation, but reveals information on the shape under consideration.
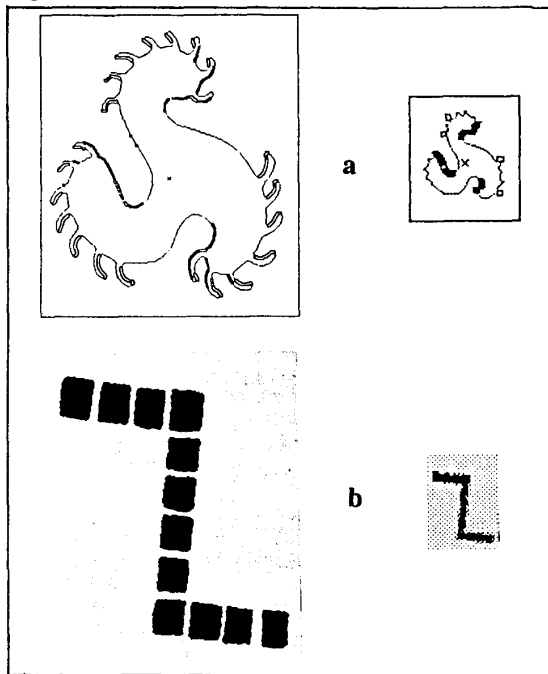

Figure 8:
Multiresolution Chirality Analysis.
a) Different chirality for general shape at low resolution and details at high resolution.
b) Disconnected object that becomes connected at lower resolution level.

The chirality at lower resolution levels describes a feature of the general shape, while chirality at higher resolution levels incorporates the features of the fine details. When the chirality of the fine details differs from the chirality of the general shape, the chirality measure can change drastically with resolution as shown in Figure 8.a . Figure 8.b shows another benefit of the multiresolution approach.

The pyramid can also help in the analysis of non connected objects. The rotational measures give desired results only on simply connected objects. When fragmented objects are given, the reduction of resolution can yield connected objects at lower resolution level, where analysis is possible. Figure 8.b shows the analysis of non-connected object at lower resolution.

6. Concluding Remarks

A measure based on rotational features of two dimensional objects has been suggested for chirality analysis. This measure is robust, and is immune to insignificant deviation and some occlusion. It has a drawback in that it works only for simply connected binary shapes, as compared to the transform and moments methods, which are theoretically applicable to every function. However, in its domain it has superior performance than the other methods.

Acknowledgment

References

[1]   - M. B. Green: Superstrings, *Scientific American*, pp. 44-56, September 1986.

[2]   - H. H. Jaffe and M. Orchin : *symmetry in chemistry*, John Wiley and Sons, New York 1965.

[3]   - R. Dubos, *Pasteur and Modern Science*, Anchor 1960.

[4]   - M. Hu : Visual Pattern Recognition by Moment Invariants, *IRE Tran. on Information Theory*, pp. 179-187, 1962.

[5]   - J. Bigun and G. Granlund : Central Symmetry Modelling, Linkoping university, internal report of the department of electrical engineering, 1986.

[6]   - A. Rosenfeld and A. C. Kak : *Digital Picture Processing*, vol. 2, Academic Press, New York, 1982.

[7]   - S. Kirpatrick and C. D. Gelatt, Jr. , M. P. Vecchi : Optimization Simulated Annealing, *science*, pp. 671-680, 13 May 1983.

[8]   - A. Rosenfeld : *Multiresolution Image Processing and Analysis*, Springer-Verlag, 1984.